Enhanced ionic conductivity in pyrochlore and fluorite mixed phase yttrium-doped lanthanum zirconate

Fan Yang [a], Yanfei Wang [a], Xiaofeng Zhao [b], Ping Xiao [a, b, *]

[a] Materials Science Centre, School of Materials, University of Manchester, Manchester M13 9PL, UK
[b] School of Materials Science and Engineering, Shanghai Jiaotong University, 800 Dongchuan Road, Shanghai 200240, PR China

HIGHLIGHTS

- Enhanced ionic conductivity in a P and F two-phase Y-doped $La_2Zr_2O_7$.
- The conductive P/F phase boundary contributes to the conductivity enhancement.
- The effect of P/F phase boundary is confirmed by FE modelling.

ARTICLE INFO

ABSTRACT

A series of yttrium-doped lanthanum zirconate $(La_{1-x}Y_x)_2Zr_2O_7$ ($0 \leq x \leq 1$) bulk samples were prepared and their ionic conductivities were studied by impedance spectroscopy. It is found that intermixing of Y and La ions increases the conductivity of the end members pyrochlore-type $La_2Zr_2O_7$ and fluorite-type $Y_2Zr_2O_7$. Highest conductivity which is 2–3 orders of magnitude higher than that of $La_2Zr_2O_7$ and $Y_2Zr_2O_7$ is achieved in a two-phase sample which consists of both pyrochlore and fluorite phases. The enhanced conductivity in the two-phase sample is attributed to the presence of the pyrochlore-fluorite phase boundary, which has higher conductivity than the pyrochlore and the fluorite phase grains. The effect of the conductive phase boundary has been confirmed by a 2-dimensional finite element modelling.

© 2014 Elsevier B.V. All rights reserved.

1. Introduction

Oxides with the formula $A_2^{3+}B_2^{4+}O_7$ could present pyrochlore structure or defect fluorite structure, depending on the ionic radius ratio $r(A^{3+})/r(B^{4+})$ [1]. They have gained considerable attention as electrolyte materials for solid oxide fuel cells (SOFCs) due to their good ionic conductivity. Many efforts have been devoted to understand the crystal structure–conductivity relationship in pyrochlore-type and fluorite-type oxides, so as to increase their conductivity to meet the requirement as electrolyte materials for intermediate temperature SOFCs [2,3].

To achieve high conductivity, the oxides must have low activation energy for migration and high concentrations of mobile vacancies, both of which are closely related to their crystal structure, where the ionic radius ratio, $r(A^{3+})/r(B^{4+})$, plays an important role. Pyrochlore-type structure is favoured when $r(A^{3+})/r(B^{4+})$ lies within the range of 1.46–1.78 [1]. The 8-coordinated A^{3+} ions are located at the 16c site, the 6-coordinated B^{4+} at the 16d site, and the O^{2-} ions at the 8a and 48f sites [4]. The 8b site is vacant in the completely ordered pyrochlore-type structure, so that the pyrochlore oxides can be intrinsic anion conductors without any dopant [5]. There exists preferential conduction paths through the cation tetrahedron plane around the 48f oxygen sites [6,7], therefore the ordered pyrochlore-type oxides usually have low activation energy. However, they have low concentration of mobile vacancy, which limits the ionic conductivity. Within the pyrochlore-type range, when the $r(A^{3+})/r(B^{4+})$ decreases, oxygen vacancies are generated at the 48f site due to the partial occupation of O^{2-} ions at the vacant 8b site [8]. Since the ionic conduction in the pyrochlore-type oxides is predominated by an oxygen vacancy-hopping mechanism between 48f sites [9], a decrease in the $r(A^{3+})/r(B^{4+})$ leads to an increase in the concentration of the mobile charge carriers, however,

---

* Corresponding author. Materials Science Centre, School of Materials, University of Manchester, Manchester M13 9PL, UK. Tel.: +44 161 3065941; fax: +44 161 3063586.
E-mail addresses: p.xiao@manchester.ac.uk, ping.xiao@manchester.ac.uk (P. Xiao).

an increase in the activation energy as well due to cation disordering. The ionic conductivity is therefore controlled by the two competing factors. Further decrease of $r(A^{3+})/r(B^{4+})$ to below 1.46 results in the formation of fluorite-type structure, in which the cations are totally disordered. The fluorite-type oxides have higher activation energy compared with the pyrochlore-type, but it decreases with an increase in $r(A^{3+})/r(B^{4+})$ due to an increase in the lattice volume [5], whereas the vacancy concentration remains constant at its maximum. As a consequence, the ionic conductivity for the fluorite-type increases with increasing $r(A^{3+})/r(B^{4+})$. Yamamura et al. [5] have concluded that the highest ionic conductivity could be achieved when $r(A^{3+})/r(B^{4+})$ lies at the vicinity of the phase boundary between pyrochlore- and fluorite-type, i.e., in $Eu_2Zr_2O_7$, $r(A^{3+})/r(B^{4+}) = 1.486$.

Up to date, many studies have reported the improvement of ionic conductivity in the pyrochlore- and fluorite-type oxides from tuning the composition by doping elements into A site [10—14], B site [15] and both [4,16,17]. More interestingly, Ou et al. [18] reported an enhanced ionic conductivity in $La_2Zr_2O_7$ nano fibers consisting of a mixed pyrochlore and fluorite phases. The enhancement is suggested to be a result of an interface lattice mismatch between the two phases, although the high surface area and the nano-size grains may also contribute to the high conductivity. Yamamura et al. [19] also observed an increased electrical conductivity in $LaY_{1-x}InO_3$ ($0.05 \leq x \leq 0.10$) which is composed of a mixed phase of B-type rare earth structure and perovskite-type structure. The authors speculated that the lattice distortion or disorder energy plays a role as driving force for the oxide-ion conduction, however, the mechanism is yet well understood. Nevertheless, the above findings provide a new strategy to achieve high conductivity of oxide ion conductors.

In this paper, the conductivity of a series of yttrium-doped lanthanum zirconate $(La_{1-x}Y_x)_2Zr_2O_7$ ($0 \leq x \leq 1$) was studied. The samples change from pure pyrochlore phase, a mixture of pyrochlore and fluorite phases, to pure fluorite phase with the composition factor from 0 to 1, so that the effect of doping on each individual phase and most importantly, the effect of the pyrochlore/ fluorite phase boundary of the two-phase samples could be investigated. The effect of phase boundary was discussed and confirmed by a 2-dimensional finite element modelling. Our results show that improvement of ionic conductivity by generating conductive phase boundaries could be effective even in bulk materials with normal grain sizes, which provides a new method of developing candidate materials for solid electrolyte with high conductivity.

2. Experiments

The powders of the samples were prepared by a co-precipitation/calcination method. Starting materials of La(N-O$_3$)$_3$·6H$_2$O (Sigma Aldrich, UK), ZrO(NO$_3$)$_2$·6H$_2$O (Sigma Aldrich, UK) and Y(NO$_3$)$_3$·6H$_2$O (Sigma Aldrich) were weighed according to the target composition of $(Y_xLa_{1-x})_2Zr_2O_7$ ($0 \leq x \leq 1$). The mixtures of the above salts were dissolved in distilled water and magnetically stirred for 24 h, and then added into aqueous ammonia solution. The precipitate was filtered, washed with distilled water and ethanol, dried in air for 24 h and then calcined at 1200 °C for 12 h. The resulting product was further milled by attrition milling in distilled water for 12 h and then freeze-dried to obtain the final powders with the designed compositions. Finally, the final powder products were pressed into tablets by a uniaxial cold pressing under 100 MPa and then sintered at 1600 °C for 2 h in air.

The phase compositions of the sintered pellets were identified by X-ray diffraction (XRD, Philips X'Pert) with CuKα radiation. The measurements were performed on the polished sample surfaces

with a step scanning mode (step size of 0.05°). The lattice parameters were calculated from a slow scan of the $(622)_P/(311)_F$ peak of the sintered pellets using the least-squares method. The microstructure of the sintered pellets was observed by scanning electron microscope (SEM, Philips XL30).

Electrical properties of the samples were obtained from ac impedance spectroscopy measurement using a Solatron SI 1255 HF frequency response analyser coupled with a Solatron 1296 Dielectric Interface (Solartron, UK). Silver paint was coated on the polished surfaces of the samples and fired at 690 °C for 0.5 h in air to serve as electrodes. During impedance measurements, an alternative current (ac) voltage of 0.1 V was applied to the sample over a frequency range from 0.1 to 10^7 Hz. The measurements were carried out during heating from 400 to 600 °C. The oxygen partial pressure $P(O_2)$ dependence of conductivity was also measured. The samples were placed inside a closed tube furnace. $P(O_2)$ was achieved by mixing oxygen-free nitrogen (BOC, UK) and air (BOC, UK), and varied from 10^{-3} to 0.22 atm. After measurements, all the spectra were fitted by an equivalent circuit using Zview Impedance Analysis software (Scribner Associates, Inc., Southern Pines, NC).

Finite element modelling was carried out using COMSOL 3.3 software coupled with Matlab. Fundamentals of the application of the finite element method in impedance spectra simulation can be found in Ref. [20]. Descriptions of the boundary conditions and calculation procedures can be found in Refs. [20,21]. Geometric models and physical parameters used for the modelling will be described in part 4.2.

3. Results

Fig. 1(a) shows the XRD patterns of the sintered $(La_{1-x}Y_x)_2Zr_2O_7$ ($0 \leq x \leq 1$) pellets. $La_2Zr_2O_7$ ($x = 0$) has a single pyrochlore phase, as indicated by the superstructure peaks of (331) and (511) due to cation ordering. The single pyrochlore phase can be maintained in the solid solutions with an increase in x up to 0.4. Further increase in x from 0.4 to 0.7 leads to a two-phase region, where both pyrochlore and fluorite phases are present. Single fluorite phase is observed in the samples when $0.8 \leq x \leq 1$.

Fig. 1(b) shows the plot of lattice parameter against composition of the $(La_{1-x}Y_x)_2Zr_2O_7$ ($0 \leq x \leq 1$) pellets. For single pyrochlore phase and fluorite phase ($0 \leq x \leq 0.4$ and $0.8 \leq x \leq 1$), the lattice parameter decreases linearly with an increase in x, which is in agreement with the Vegard's law for cubic systems, as indicated by the dash line in the figure. The linear decrease of the lattice parameter is related to the substitution of La^{3+} ions ($r = 1.16$ Å [22]) by smaller Y^{3+} ions ($r = 1.019$ Å [22]). In the two-phase region ($0.5 \leq x \leq 0.7$), the lattice parameter for each phase remains constant, as indicated by the horizontal lines. The compositions of the two-phase samples could be estimated to be $(La_{0.6}Y_{0.4})_2Zr_2O_7$ for the pyrochlore phase and $(La_{0.2}Y_{0.8})_2Zr_2O_7$ for the fluorite phase according to their lattice parameters. The lattice parameters and the compositions for the two-phase samples are in general agreement with the results reported in Ref. [8].

The mass fraction of the pyrochlore and the fluorite phase in the two-phase region was estimated by the Klug equation [23]:

$$f_P = \frac{I_P^{mix} / I_P^{pure}}{A_P - \left(I_P^{mix}/I_P^{pure}\right) \cdot (A_P - A_F)}, \tag{1}$$

where f_P is the mass fraction of the pyrochlore phase; I_P^{mix} and I_P^{pure} represent the intensity of the (222) peak of the pyrochlore phase in the mixture and in the pure phase, respectively; A_P and A_F are the mass absorption coefficient of each phase, which are calculated based on the compositions of $(La_{0.6}Y_{0.4})_2Zr_2O_7$ for pyrochlore phase
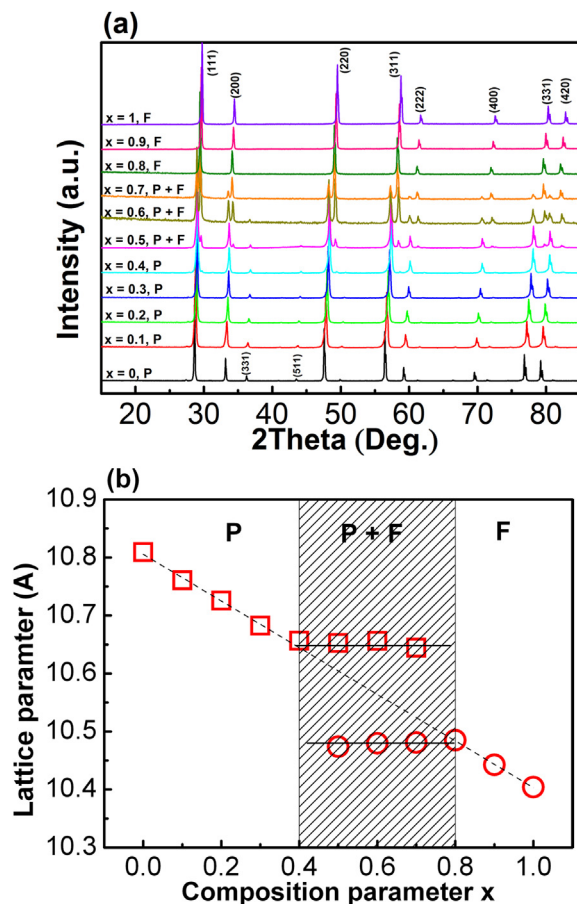
Fig. 1. (a) XRD patterns and (b) lattice parameters of the sintered $(La_{1-x}Y_x)_2Zr_2O_7$ ($0 \leq x \leq 1$) pellets. The square and circle symbols represent the lattice parameters of the pyrochlore phase and the fluorite phase, respectively. For the fluorite phase, the lattice parameters are doubled to keep consistency with the pyrochlore phase. The dash line indicates the lattice parameters predicted by the Vegard's law.

and $(La_{0.2}Y_{0.8})_2Zr_2O_7$ for fluorite phase using the mass absorption coefficient values for Y, La, Zr and O elements at 8.04 KeV according to $A = \sum x_i A_i$, where x_i is the mass fraction of each element in the compound. The mass fraction of each phase in the two-phase samples is listed in Table 1. As the densities of the two phases are close, i.e., 5.83 g cm^{-3} for the pyrochlore phase and 5.64 g cm^{-3} for the fluorite phase, the volume fraction is almost identical to the mass fraction.

The SEM images of the sintered pellets (Fig. 2) show that the samples are almost fully-dense, thus the porosity effect is negligible in this study. The end members, $La_2Zr_2O_7$ ($x = 0$) and $Y_2Zr_2O_7$ ($x = 1$) have large grains with an average size of ~5 μm. Samples with composition factors of $0.3 \leq x \leq 0.7$ have relatively smaller grains. The grain size varies from 0.5 to 2 μm in each sample.

Fig. 3 shows the impedance spectra of the samples measured at 500 °C. When $0 \leq x \leq 0.2$, only one semicircle is shown on the Nyquist plot (Fig. 3(a) and (b)); When $0.3 \leq x \leq 1$, two semicircles are displayed on the Nyquist plot (Fig. 3(c) to (f)). For the single

Table 1
Mass fraction of each phase in the two-phase samples.

Composition factor x	Pyrochlore phase	Fluorite phase
0.5	82%	18%
0.6	41%	59%
0.7	27%	73%

phase samples, the two semicircles represent the responses from the bulk (grains) and the grain boundaries, respectively. For the two-phase samples ($x = 0.5$ and 0.7), the electric current could be impeded by the grains and grain boundaries of both phases, as well as the pyrochlore/fluorite phase boundaries. The high frequency (HF) or the low frequency (LF) semicircle may include contribution from the pyrochlore/fluorite phase boundary, depending on its conductivity. The details will be further discussed in part 4.2. The impedance spectra were fitted by equivalent circuits of one parallel-aligned resistance-constant phase element (R-CPE) for $0 \leq x \leq 0.2$ and two R-CPE in series connection for $0.3 \leq x \leq 1$. The fitting parameters for all the samples measured at 500 °C are listed in Table 2.

The conductivity of the high frequency response and the total conductivity were calculated from the resistances by.

$$\sigma_{HF} = \frac{1}{R_{HF}} \frac{4t}{\pi D^2}, \tag{2}$$

and.

$$\sigma_{total} = \frac{1}{R_{HF} + R_{LF}} \frac{4t}{\pi D^2}, \tag{3}$$

where t and D represent the thickness and the diameter of each pellet.

The composition dependence of the conductivity of the high frequency response is shown in Fig. 4(a). For the single pyrochlore phase ($0 \leq x \leq 0.4$), the conductivity of the high frequency response represents the bulk (grain) conductivity. It increases with an increase in x, indicating the substitution of La^{3+} by Y^{3+} is beneficial to achieve high conductivity. For the single fluorite phase ($0.8 \leq x \leq 1$), the conductivity of the high frequency response decreases with increasing x, suggesting the substitution of Y^{3+} by La^{3+} is also beneficial to the improvement of conductivity. The highest conductivity is obtained in the sample with a composition factor $x = 0.5$, which consists of 82% pyrochlore and 18% fluorite phases. The total conductivity calculated from Eq. (3) shows similar trend that it goes up till $x = 0.5$ and then decreases with further increase in the composition factor, as shown in Fig. 4(b).

The temperature dependence of the conductivity is described by:

$$\sigma = \frac{\sigma_0}{T} \exp\left(-\frac{E_a}{k_B T}\right), \tag{4}$$

where E_a is the activation energy, σ_0 is the pre-exponential factor, T is the absolute temperature and k_B is the Boltzman constant. Fig. 5(a) shows the variation of σ_0 and E_a of the high frequency response as a function of the composition factor x. The pre-exponential factor, σ_0, shows a monotonically increase with an increase in the composition factor, whereas the $E_a −x$ relationship exhibits more features. For $0 \leq x \leq 0.2$, E_a remains around 0.85 eV. A drop of E_a to 0.7 eV is noticed when $x = 0.3$, and then E_a increases smoothly with an increase in x to 1 eV till $x = 0.7$. Further, E_a jumps to 1.2 eV at the start of the single fluorite phase region $x = 0.8$, and then increases progressively in the single fluorite phase region. It is worth mentioning that $x = 0.3$ is the composition that two semicircles start to be observed on the Nyquist plot. The drop of E_a at $x = 0.3$ leads to the speculation that the higher E_a for $0 \leq x \leq 0.2$ is possibly due to the fact that the only semicircle on the Nyquist plot might include grain boundary contribution. Within this composition range, grain and grain boundaries have similar time constant, so their responses could not be well resolved from the impedance spectra. This speculation is not unreasonable as the E_a for total conductivity, as shown in Fig. 5(b), exhibits a steadily increase from

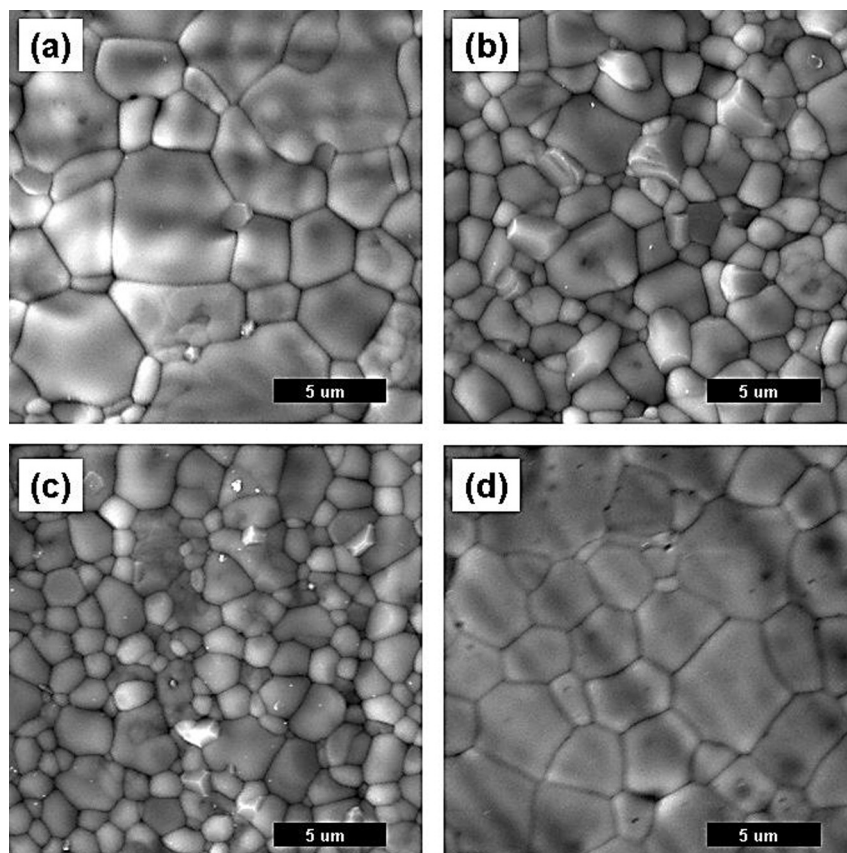**Fig. 2.** SEM images of the $(La_{1-x}Y_x)_2Zr_2O_7$ ($0 \leq x \leq 1$) pellets. (a) $x = 0$; (b) $x = 0.3$; (c) $x = 0.7$ and (d) $x = 1$.

$x = 0.2$ to 0.3. However, to confirm this hypothesis needs further investigation, which is beyond the scope of the present paper. It is also noticed that that E_a increases less rapidly in the two-phase region than in the single fluorite phase region, which might related to the pyrochlore/fluorite phase boundary.

Fig. 6(a) and (b) show the effect of oxygen partial pressure $P(O_2)$ on the conductivity of the high frequency response and the total conductivity for a two-phase sample, $x = 0.7$, measured at 400, 500 and 600 °C. The conductivity is independent on the oxygen partial pressure, indicating that ionic conduction is dominated within the temperature and the $P(O_2)$ range. Samples with other composition factors, no matter single-phase or two-phase, also have $P(O_2)$-independent conductivities, as shown in Fig. 6(c) and (d). Therefore, in this study, the conduction mechanism for all the samples is dominated by ionic conduction, hole or electronic conduction could be ruled out within the studied temperature and $P(O_2)$ range.

4. Discussion

4.1. Doping effect in the single-phase samples

In the single pyrochlore phase region, $0 \leq x \leq 0.4$, the bulk conductivity increases with an increase in x, which can be mainly due to a significant increase in the pre-exponential factor σ_0, as shown in Fig. 5(a). The substitution of La^{3+} by smaller Y^{3+} results in a partial occupation of the 8b site by O^{2-} ions, so that oxygen vacancies are generated at the 48f site. Whittle et al. [8] reported an increase in the 8b site occupancy with an increase in the yttrium dopant content in the pyrochlore phase $La_2Zr_2O_7$, hence a larger number of mobile vacancy at the 48f site. An increase in the charge

carrier concentration is the dominant factor for the enhancement of conductivity for the pyrochlore phase region.

In the single fluorite phase region, $0.8 \leq x \leq 1$, the introduction of La^{3+} ions into $Y_2Zr_2O_7$ also has a positive effect on the conductivity. Substitution of Y^{3+} by larger La^{3+} ions increases the lattice parameter, and thus increases the radius of the free channel for charge carriers to migrate [24] and lowers the activation energy. Therefore, in the fluorite phase region, the enhanced conductivity is mainly benefited from a drop in the activation energy.

To sum up, for the single pyrochlore phase, the conductivity increases with a decrease in $r(A^{3+})/r(B^{4+})$; for the single fluorite phase, the conductivity increases with an increase in $r(A^{3+})/r(B^{4+})$. The present results are in consistence with the findings in Ref. [5].

4.2. Phase boundaries in the two-phase samples

In a two-phase sample, the electric current can be impeded by the grains and grain boundaries from both phases, as well as the pyrochlore/fluorite phase boundaries. Grain boundaries are known to be more resistive than grains, i.e., the grain boundary conductivity is usually two or three orders of magnitude lower than the bulk conductivity either due to impurity segregation or space charge effect [25]. The conductivity of the pyrochlore/fluorite phase boundaries is yet unknown. Theoretically, it could be obtained from the impedance spectroscopy if the response from the phase boundaries can be distinguished from other responses. i.e., from the grains and the grain boundaries of each phase, however, as shown in Fig. 3(d) and (e), the existence of the phase boundaries does not add additional features to the impedance spectroscopy. This indicates that the relaxation frequency of the phase boundary is close
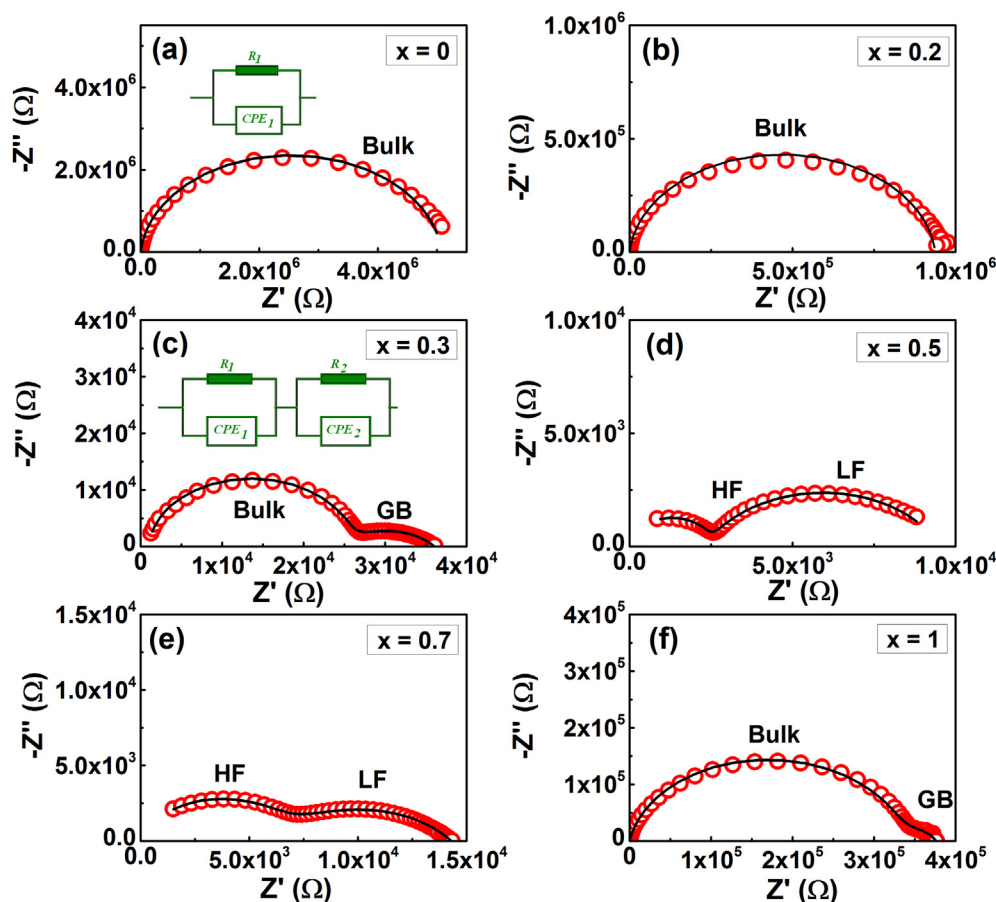
Fig. 3. Impedance spectra (Nyquist plots) of selected samples measured at 500 °C. (a) $x = 0$, (b) $x = 0.2$, (c) $x = 0.3$, (d) $x = 0.5$, (e) $x = 0.7$ and (f) $x = 1$. The red hollow circles represent the measured data, while the black solid lines represent the equivalent circuit fitting results. The inset figure in (a) is the equivalent circuit used to fit data of (a) and (b), and the inset in (c) is the equivalent circuit used to fit data of (c) to (f). All the impedance data have been normalised to an electrode area of 1 cm^2 and a thickness of 1 mm for comparison. (For interpretation of the references to colour in this figure legend, the reader is referred to the web version of this article.)

to any of the other responses, and therefore causes overlap of the semicircles on the Nyquist plot.

As stated in Part 3, for the two-phase samples, the composition of each phase is $(La_{0.6}Y_{0.4})_2Zr_2O_7$ (pyrochlore) and $(La_{0.2}Y_{0.8})_2Zr_2O_7$ (fluorite), in which the pyrochlore phase has higher conductivity than the fluorite phase according to Fig. 4(a). For a composite material, the conductivity usually lies in between the conductivity of each component. However, it is noticed that the sample with composition factor $x = 0.5$, which consists of 82% pyrochlore phase

Table 2
Equivalent circuit fitting parameters for the samples measured at 500 °C. The data are normalised to an electrode area of 1 cm^2 and a thickness of 1 mm for comparison.

Composition factor x	High frequency (HF) arc			Low frequency (LF) arc		
	R_1 (Ω)	Q_1	n_1	R_2 (Ω)	Q_2	n_2
0	5.12×10^6	2.59×10^{-11}	0.95	–	–	–
0.1	2.39×10^6	5.73×10^{-11}	0.95	–	–	–
0.2	9.37×10^5	5.52×10^{-11}	0.95	–	–	–
0.3	2.42×10^4	2.86×10^{-11}	0.98	7.57×10^3	7.36×10^{-6}	0.57
0.4	3.29×10^3	3.41×10^{-11}	1	6.91×10^3	1.56×10^{-7}	0.71
0.5	2.34×10^3	4.25×10^{-11}	1	5.83×10^3	8.49×10^{-8}	0.75
0.6	4.10×10^3	2.75×10^{-10}	0.86	6.63×10^3	2.12×10^{-7}	0.58
0.7	6.39×10^3	1.01×10^{-9}	0.81	8.29×10^3	5.18×10^{-7}	0.58
0.8	3.84×10^4	1.82×10^{-9}	0.73	2.62×10^4	4.38×10^{-7}	0.51
0.9	1.99×10^5	1.67×10^{-10}	0.89	8.90×10^4	4.00×10^{-7}	0.75
1	3.33×10^5	1.26×10^{-10}	0.90	4.08×10^4	1.23×10^{-7}	0.75

and 18% fluorite phase, has a higher conductivity than its conductive pyrochlore phase component. This could be related to the existence of the pyrochlore/fluorite phase boundary. However, the response from the phase boundaries cannot be extracted from the impedance spectra.

In order to obtain the conductivity of the phase boundaries, finite element modelling was employed to simulate the impedance spectrum of the two-phase samples. As shown in Fig. 7(a), the microstructure of the two-phase sample was simplified into a 10×10 array of equal-size squares according to the brick-layer model [26] for crystalline materials. Each square with a side length of 1 μm was numbered from 1 to 100. The positions of the second phase (fluorite) grains were determined using the random number generator in Matlab. The grains of each phase were separated by thin layers of grain boundaries and phase boundaries. To simulate the sample with small grains, as well as to reduce the difficulty in meshing too small components and too thin layers, the grain boundary and the phase boundary were treated as thin layers with thickness 1/10 of the grain size.

Fig. 7(b) presents the calculated impedance spectra of the model in Fig. 7(a). Two semicircles are present on the calculated Nyquist plot. When the phase boundary conductivity, σ_{PB}, varies from 0.1 S m^{-1} to 0.01 S m^{-1}, the high frequency semicircle becomes larger, which suggests that the phase boundary contributes to the high frequency response besides the grains of each phase, which confirms the fact that the enhanced conductivity of the high frequency response is attributed to the phase boundary. The
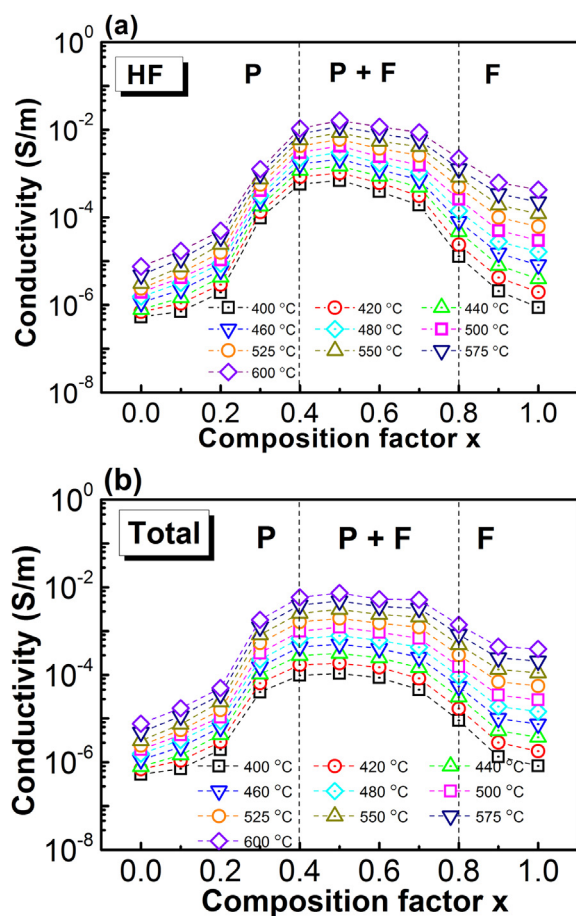
Fig. 4. Composition dependence of the (a) conductivity of the high frequency (HF) response and (b) total conductivity at various temperatures from 400 to 600 °C.

Fig. 5. Activation energy and pre-exponential factor for (a) the conductivity calculated from the high frequency (HF) response and (b) total conductivity.

impedance spectra can be fitted by an equivalent circuit of two R-CPE elements in series connection to obtain the conductivity of the high frequency response.

Using the method described above, a series of models with the second phase fraction varying from 0 to 100% were established. The conductivity of the high frequency response as a function of the second phase fraction, along with the influence of the phase boundary conductivity, was obtained, as shown in Fig. 8. The calculation results show that the conductivity of the phase boundary has to be at least one order of magnitude higher than the conductivity of the pyrochlore phase grains to notice an increase in the conductivity of the high frequency response. In the current case, the second phase (fluorite) has a lower conductivity than the pyrochlore phase. Without contribution from highly conductive phase boundaries, the conductivity of the high frequency response should decreases with increasing fluorite phase fraction. On the other hand, if the fluorite phase has similar conductivity with the pyrochlore phase, then the highest conductivity should be obtained when there is maximum amount of pyrochlore/fluorite phase boundary, i.e., when there is equal amount of pyrochlore and fluorite phase (50%). Therefore, the conductivity of the high frequency response is an overall effect from the highly conductive pyrochlore/fluorite phase boundary and the less conductive fluorite phase grains. The experimental result shows the best fit with the calculated conductivity when $\sigma_{PB} = 0.1$ S m^{-1}. Due to the simplification of the geometric model, the σ_{PB} value is only suggestive. However, the agreement between the finite element calculations and the experimental results confirms the contribution of the highly conductive pyrochlore/fluorite phase boundary to the high frequency response.
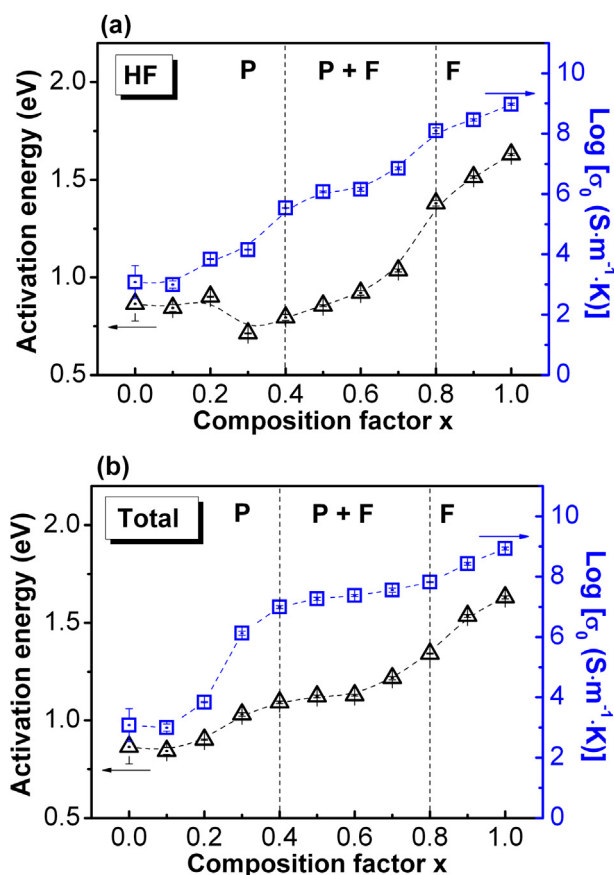
4.3. Possible reason of the conductive pyrochlore/fluorite phase boundary

High ionic conductivity at the interface in a heterostructure has been observed in some multilayer thin films [27–32]. The increased conductivity at the heterophase is usually interpreted by the lattice strain or misfit dislocations generated due to the lattice mismatch of the two materials, which provide a fast pathway for the migration of oxygen ions.

The pyrochlore/fluorite phase boundary is the interface of two ion-conducting oxides. Due to the similarity in the crystal symmetry (cubic structure) and commensurable lattice parameters (10.645 Å for the pyrochlore phase and 10.484 Å for the fluorite phase), coherent interfaces can be formed at the phase boundary [33]. The lattice parameter of the pyrochlore phase is larger than the fluorite phase. Consequently, the pyrochlore phase will be under compressive strain, whereas the fluorite phase will be under tensile strain. The lattice strain relative to the pyrochlore phase, ε_P, can be calculated by Ref. [33]:

$$\varepsilon_P = \frac{a_P - a_F}{a_P}, \tag{5}$$

where a_P and a_F represent the lattice parameter for the pyrochlore and the fluorite phase, respectively. The Young's modulus of the pyrochlore phase is ~200 GPa [34], so the estimated compressive stress in the pyrochlore phase at the interface is ~3 GPa. Zhang et al.
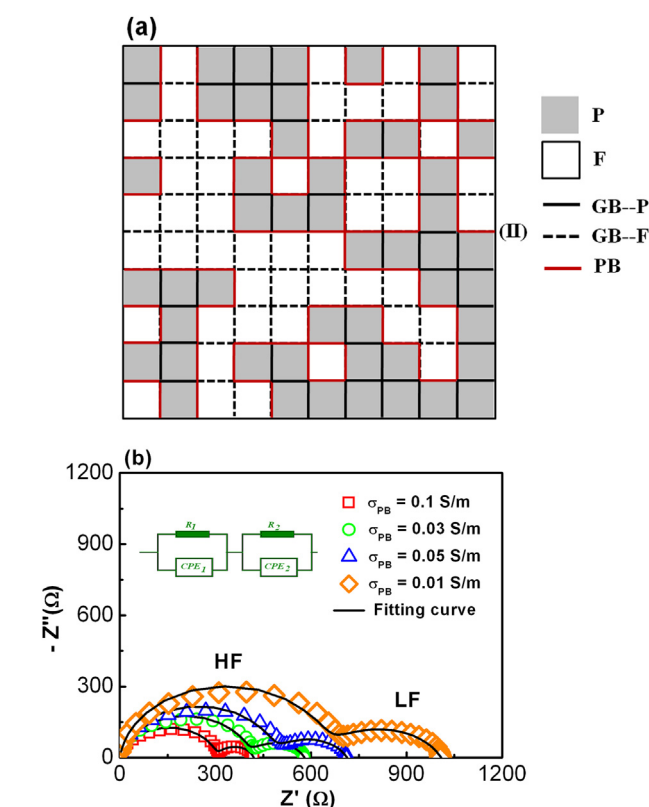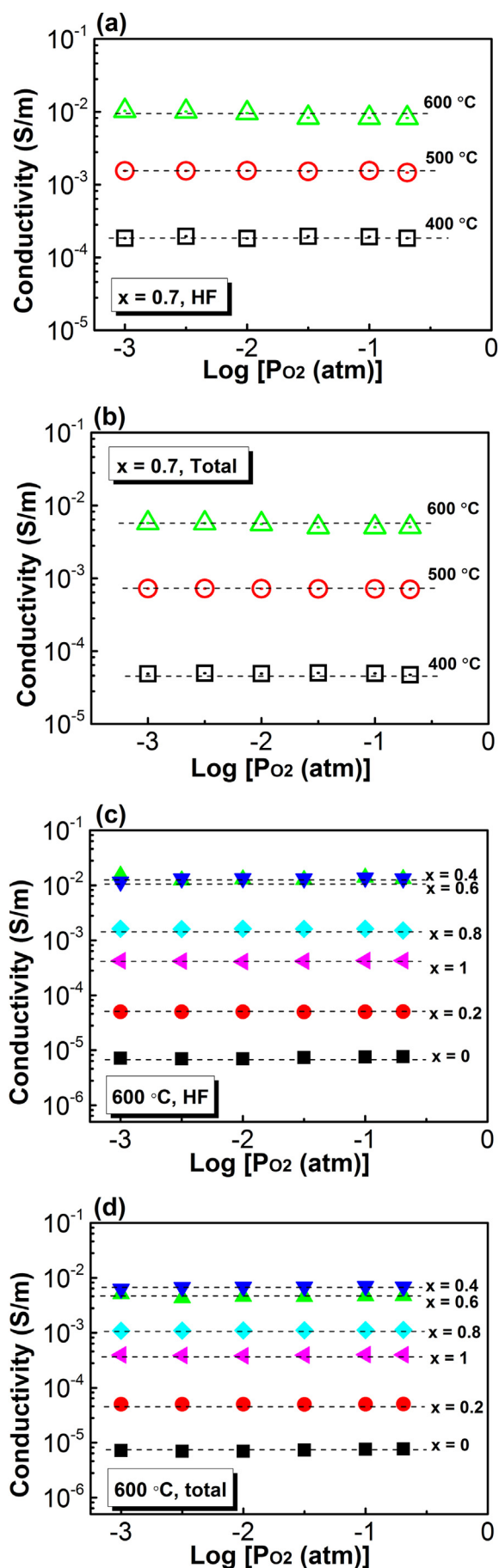
Fig. 7. (a) A 2-dimensional geometric model for a two-phase sample with 50% pyrochlore phase and 50% fluorite phase. The grey and white squares represent the grains for the pyrochlore phase and the fluorite phase, respectively. The black solid lines represent the grain boundaries of the pyrochlore phase, and the black dash lines represent the grain boundaries of the fluorite phase. The red solid lines represent the pyrochlore/fluorite phase boundaries. (b) The calculated Nyquist plot and the equivalent fitting curve. The physical parameters used in the calculations are: $\sigma_P = 3.0 \times 10^{-3}$ S m^{-1}, $\sigma_{P-GB} = 5.0 \times 10^{-6}$ S m^{-1}, $\varepsilon_P = \varepsilon_{P-GB} = 80$; $\sigma_F = 3.0 \times 10^{-4}$ S m^{-1}, $\sigma_{F-GB} = 5.0 \times 10^{-7}$ S m^{-1}, $\varepsilon_F = \varepsilon_{F-GB} = 70$; $\varepsilon_{PB} = 75$. These parameters are based on the experimental results at 500 °C. (For interpretation of the references to colour in this figure legend, the reader is referred to the web version of this article.)

[35] reported a rapid decrease of the atomic coordinate, x_{48f}, in the pyrochlore-type La$_2$Zr$_2$O$_7$ when it is subjected to pressure upto 5 GPa, indicating an increase in the anion disorder. Under compression, the oxygen ions are partially removed from the 48f site to the vacant 8b site, which increases the number of mobile charge carriers, and thereby increases the ionic conductivity. From the fluorite side, the tensile stress leads to a lattice expansion at the interface, which enlarges the free channel for oxygen vacancies to move and also improves the ionic conduction.

Unlike thin films grown on single crystal substrates, the grains of bulk samples usually do not have any preferred orientation. It is also possible that the grains of the two phases with different crystallographic planes are in contact, which has large mismatch to form semi-coherent or even incoherent interfaces. In this case, the mismatch dislocations or other defects can act as fast diffusion paths or lower the activation energies for ionic transportation [28], which might be another reason for the higher conductivity at the pyrochlore/fluorite interface.

Fig. 6. Oxygen partial pressure dependence of conductivity. (a) conductivity of the high frequency (HF) response and (b) total conductivity for the two-phase sample $x = 0.7$, measured from 400 to 600 °C; (c) conductivity of the high frequency response and (d) total conductivity for the samples with different composition factors measured at 600 °C.
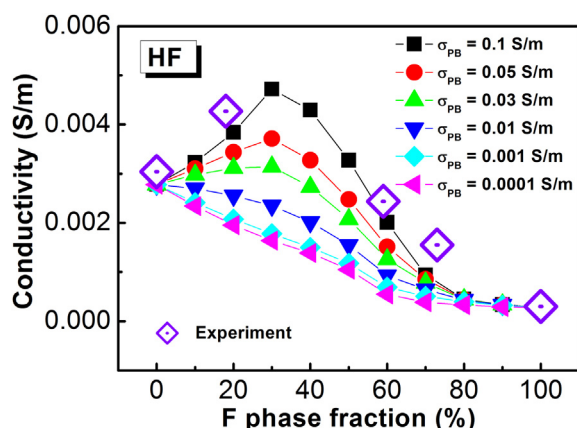
Fig. 8. Conductivity of the high frequency (HF) response for the two-phase composites as a function of the fraction of the second phase (fluorite) obtained from finite element modelling, and a comparison with the experimental values. F represents fluorite.

5. Conclusion

In this paper, a series of yttrium-doped lanthanum zirconate $(La_{1-x}Y_x)_2Zr_2O_7$ ($0 \leq x \leq 1$) were prepared and the effect of doping on the ionic conductivity was studied. Major conclusions are:

1) With an increase in the composition factor x, the samples change from single pyrochlore phase ($0 \leq x \leq 0.4$), a mixture of pyrochlore and fluorite phases ($0.5 \leq x \leq 0.7$) to single fluorite phase ($0.8 \leq x \leq 1$). The phase change is simply due to the fact that substitution of La^{3+} ions by smaller Y^{3+} ions decreases $r(A^{3+})/r(B^{4+})$ and thus destabilises the pyrochlore phase structure.

2) In the single pyrochlore phase region $0 \leq x \leq 0.4$, the ionic conductivity increases with increasing x, which is mainly due to an increase in the number of mobile oxygen vacancy at the 48f site. In the single fluorite phase region, $0.8 \leq x \leq 1$, the conductivity decreases with an increase in x, which is mainly due to an increase in the activation energy for migration.

3) The highest conductivity of the series of $(La_{1-x}Y_x)_2Zr_2O_7$ ($0 \leq x \leq 1$) is obtained in a two-phase sample when $x = 0.5$. The two-phase composite consists of 82% pyrochlore phase and 18% fluorite phase, in which the pyrochlore phase is more conductive than the fluorite phase. The high conductivity is due to the existence of a conductive pyrochlore/fluorite boundary. Finite element modelling results indicate that the conductivity of the pyrochlore/fluorite boundary is at least one order of magnitude higher than the pyrochlore phase grains.

4) The conductive pyrochlore/fluorite phase boundary could be attributed to the lattice mismatch between the two phases. At the phase boundary, the lattice of the pyrochlore phase under compression. The compressive stress increases the degree of anion disorder and thereby improves the ionic conduction.

5) To achieve the highest enhancement of conductivity utilizing the conductive pyrochlore/fluorite phase boundary, the following pre-requisite conditions should be considered. First, there should be as many phase boundaries as possible to highlight the effect of the conductive phase boundary. Second, the components of the two-phase composite should have similar conductivity to avoid overshadowing the phase boundary effect by the less conductive second phase.

Acknowledgement

References

[1] M.A. Subramanian, G. Aravamudan, G.V. SubbaRao, Prog. Solid State Chem. 16 (1983) 55–143.
[2] J.W. Fergus, J. Power Sources 162 (2006) 30–40.
[3] S. Hui, J. Roller, S. Yick, X. Zhang, C. Deces-Petit, Y. Xie, R. Maric, D. Ghosh, J. Power Sources 172 (2007) 493–502.
[4] H. Yamamura, H. Nishino, K. Kakinuma, K. Nomura, Solid State Ionics 178 (2007) 233–238.
[5] H. Yamamura, H. Nishino, K. Kakinuma, K. Nomura, Solid State Ionics 158 (2003) 359–365.
[6] A.J. Burggraaf, T. van Dijk, M.J. Verkerk, Solid State Ionics 5 (1981) 519–522.
[7] M.P. van Dijk, K.J. de Vries, A.J. Burggraaf, Solid State Ionics 9-10 (1983) 913–920.
[8] K.R. Whittle, L.M.D. Cranswick, S.A.T. Redfern, I.P. Swainson, G.R. Lumpkin, J. Solid State Chem. 182 (2009) 442–450.
[9] P.J. Wilde, C.R.A. Catlow, Solid State Ionics 112 (1998) 173–183.
[10] Z. Liu, J. Ouyang, Y. Zhou, X. Xia, J. Power Sources 185 (2008) 876–880.
[11] X. Xia, Z. Liu, J. Ouyang, J. Power Sources 196 (2011) 1840–1846.
[12] J.A. Diaz-Guillen, M.R. Diaz-Guillen, K.P. Padmasree, A.F. Fuentes, J. Santamaria, C. Leon, Solid State Ionics 179 (2008) 2160–2164.
[13] J.A. Diaz-Guillen, A.F. Fuentes, M.R. Diaz-Duillen, J.M. Almanza, J. Santamaria, C. Leon, J. Power Sources 186 (2009) 349–352.
[14] X. Xia, J. Ouyang, Z. Liu, S. Gao, S. Li, J. Electrochem. Soc. 157 (2010) B470–B476.
[15] X. Xia, Z. Liu, J. Ouyang, S. Gao, X. Liu, Solid State Sci. 13 (2011) 1328–1333.
[16] Z. Liu, J. Ouyang, K. Sun, Fuel Cells 2 (2011) 153–157.
[17] Z. Liu, J. Ouyang, Y. Zhou, X. Xia, Phil. Mag. Lett. 90 (2010) 753–761.
[18] G. Ou, W. Liu, L. Yao, H. Wu, W. Pan, J. Mater.Chem. A 2 (2014) 1855–1861.
[19] H. Yamamura, K. Yamazaki, K. Kakinuma, K. Nomura, Solid State Ionics 150 (2002) 255–261.
[20] J. Fleig, J. Maier, Electrochim. Acta 41 (1996) 1003–1009.
[21] L. Deng, Y. Xiong, P. Xiao, Surf. Coat. Technol. 201 (2007) 7755–7763.
[22] R.D. Shannon, Acta Cryst. A32 (1976) 751–767.
[23] L. Alexander, H.P. Klug, Anal. Chem. 20 (1948) 886–889.
[24] P.V. Ananthapadmanabhan, N. Venkatramani, V.K. Rohatgi, A.C. Momin, K.S. Venkateswarlu, J. Euro. Ceram. Soc. 6 (1990) 111–117.
[25] X. Guo, R. Waser, Prog. Mater. Sci. 51 (2006) 151–210.
[26] J.R. MacDonald, Impedance Spectroscopy- Emphasizing Solid Materials and Sytems, John Wiley & Sons, New York, USA, 1987.
[27] I. Kosacki, C.M. Rouleau, P.F. Becher, J. Bentley, D.H. Lowndes, Solid State Ionics 176 (2005) 1319–1326.
[28] A. Peters, C. Korte, D. Hesse, N. Zakharov, J. Janek, Solid State Ionics 178 (2007) 67–76.
[29] J. Garcia-Barriocanal, A. Rivera-Calzada, M. Varela, Z. Sefrioui, E. Iborra, C. Leon, S.J. Pennycook, J. Santamaria, Science 321 (2008) 676–680.
[30] M. Kubicek, Z. Cai, W. Ma, B. Yildiz, H. Hutter, J. Fleig, ACS Nano 7 (2013) 3276–3286.
[31] J.W. Han, B. Yildiz, Energy Environ. Sci. 5 (2012) 8598–8607.
[32] C. Korte, N. Schichtel, D. Hesse, J. Janek, Monatsh Chem. 140 (2009) 1069–1080.
[33] E. Fabbri, D. Pergolesi, E. Traversa, Sci. Technol. Adv. Mater. 11 (2010) 054503.
[34] Y. Wang, F. Yang, P. Xiao, Acta Mater. 60 (2012) 7024–7033.
[35] F.X. Zhang, M. Lang, Z. Liu, R.C. Ewing, Phys. Rev. Lett. 105 (2010) 015503.